Influence of lateral species diffusion and heat transfer on the evaluation of near-threshold sooting flames

Ahmad Saylam, Torsten Endres, Christof Schulz

Contents

Influence of lateral species diffusion and heat transfer on the evaluation of near-threshold sooting flames

Ahmad Saylam, Torsten Endres, Christof Schulz

EMPI, Institute for Energy and Materials Processes – Reactive Fluids, and CENIDE, Center for Nanointegration Duisburg-Essen, University of Duisburg-Essen, Duisburg, Germany

Abstract

Premixed flat flames provide an ideal platform for investigation of soot formation by optical diagnostics. The local conditions can, however, be strongly affected by species diffusion and heat transfer perpendicular to the flow direction. This work investigates the influence of the burner geometry and shielding of the target flame by a nitrogen coflow or by a surrounding non-sooting fuel-rich methane/air flame. The analysis is based on 2D simulations as well as measurements of temperature and species concentration profiles at atmospheric pressure and 10 bar. The simulations indicate that the deviation from the ideal case caused by species diffusion and heat transfer is especially strong at near-threshold sooting conditions investigated in ethylene/air flames with an equivalence ratio $\phi = 2.1$ and methane/air flames at $\phi = 1.82$. The influence of species diffusion and heat transfer on the axial temperature and species concentration profiles is considerable at atmospheric pressure and becomes lower at 10 bar. Quasi unchanged axial profiles of temperature and soot volume fraction are observed for burner diameters of ≥ 40 mm shielded by a non-sooting flame and for ≥ 60 mm shielded by a nitrogen coflow. The measured soot volume fraction profiles of different ethylene/air $\phi = 2.1$ flames with diameters of 20 and 60 mm and oxygen-containing or inert shielding coflows show almost no difference at low heights above the burner (i.e., ≤ 14 mm) but become significant at larger heights, especially for the low diameter 20 mm of flame with nitrogen as shielding coflow.

Keywords: Soot threshold, species diffusion, flat flame, one-dimensional simulation, combustion evaluation.

1. Introduction

Premixed flat flames are often used to study species and soot formation in the laboratory and to support the development of detailed reaction mechanisms. Ideally, such flames provide reaction environments where conditions change in one dimension only, often referred to as "height above burner", HAB. Radial variation in species concentrations and temperatures is therefore expected to be negligible. For the most frequently used McKenna burner, Migliorini et al. [1] showed that for studies with rich premixed ethylene/air flames, the 1D situation, and even axial symmetry is not reached. Since flat flames are stabilized by heat transfer to the matrix, temperature inhomogeneities in the burner matrix affect the geometry of the flame. In studies of the influence of the burner diameter on methane/air flames by Chander et al. [2], it was concluded that the heat flux distribution was directly related to the shape and the size of the flame. On the other hand, the surrounding environment affects the flame through diffusion, where the transport of oxygen is of special interest in rich mixtures modifying the local fuel/air equivalence ratio related to the feed gases provided to the burner. Increasing the diameter of the burner to an extent that species diffusion and heat transfer from the environment that we call "lateral" in this paper do not affect the gas composition in the center of the flame is usually not possible. Therefore, the investigation of sooting flames requires the shielding against the influence of the surroundings and – in case, such an influence cannot be avoided – methods must be derived to calculate the influence and thus determine the actual conditions along the center line. While such a flame can then no longer be simulated based on 1D models, also measurement methods that derive information from line-of-sight measurements must be carefully considered.

In this paper, we study the influence of the burner diameter and shielding by inert and reactive coflows on the evaluation of combustion products and temperature of a sooting premixed flame. This will be applied here to the methane/air and ethylene/air flames that are operated at and slightly above the threshold of soot formation of ϕ = 1.82 and 2.1, respectively, similar to the conditions previously investigated in Refs. [3, 4].

In sooting flames, the partial pyrolysis of a parent fuel under fuel-rich conditions leads to the formation of soot precursors such as acetylene and benzene, leading to the formation of polycyclic aromatic hydrocarbons (PAHs). This process is often described based on gas-phase chemical kinetics mechanisms that provide species input to modeling the subsequent soot formation. The species growth eventually leads to soot nucleation – one of the least understood steps in soot formation. Detailed studies of incipient soot formation in rich premixed flames have been done by Desgroux et al. [5-7]. This process occurs close to the flame front. At sub-atmospheric pressure, the zone of incipient soot formation is further enlarged and therefore easier to spatially resolve experimentally.

Temperature is known to have a strong influence on soot formation leading to specific temperature regimes that favor soot formation. The temperature influence on the soot yield is especially strong at the low- and high-temperature threshold of the so-called bell-shaped curve that describes the soot yield as a function of temperature [8, 9]. In the early soot formation zone, where the flame temperature is low, small aromatics and PAHs are formed in larger amounts, but the low temperature hinders the reactive inception of these species and aliphatic radicals to condense into first nuclei [10]. At higher temperatures, oxidation is very active in the secondary oxidation zone of the flame, thus destroying PAHs that are then not available for formation of larger species. Consequently, soot inception is reduced and only particularly stable structures such as graphene are formed [11, 12]. In the intermediate temperature range, the temperature is ideal for the formation of PAHs and their transformation to soot particles [8].

Many studies of premixed combustion utilize flat-flame burners with a sintered porous plate for flame stabilization and anchoring. At higher pressures, strong heat fluxes can deteriorate sinter plates over time, even when internally cooled. In addition, the porous matrix needs to be very homogeneous to avoid the formation of luminous soot streaks (i.e., inhomogeneous gaseous flow through the matrix) to appear [13]. Furthermore, the fresh gas flow has important influence on flame stability. If the gas inlet-velocity is too high, the flame can become turbulent. When it is too low, the flame is unstable and may extinguish due to too much heat loss to the burner surface. Under such conditions, stagnation plates can be used for flame stabilization through reducing buoyancy effects [14].

To reduce the influence of the surrounding oxygen on the studied flame, two approaches are often employed. The more common one is to shield the flame by an inert-gas coflow at flow velocities comparable to those of the hot burned gases [15]. The second, which also limits heat transfer to the environment is to protect the target flame by a co-annular flame, e.g., a slightly fuel-rich non-sooting methane/air flame [16-21]. Such a co-annular flame therefore enables temperature profiles with less steep or even vanishing gradients at the transition between inner and outer flame. To illustrate such a case with a simple example of non-reactive diffusive mixing of gaseous flows exiting this kind of co-annular burner geometry, Fig. 1 depicts radial species profiles at increasing HAB of two fuels (C_2H_4 and CH_4, both diluted in nitrogen) and Ar through the inner and outer burner and the co-flow, respectively, at representative temperatures of a premixed flame (1500 K) and a room temperature co-flow (300 K), respectively. Simulations were performed with a standard CFD-solver (see below) showing increased diffusive mixing when HAB increases.

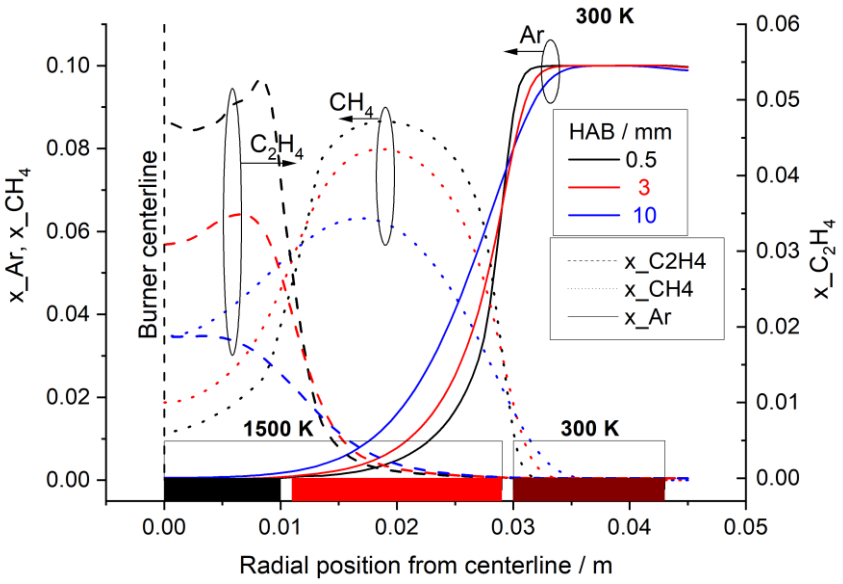

Figure 1: CFD-simulations of atmospheric pressure diffusive mixing of three species (C_2H_4, CH_4, Ar) as representative tracer species exiting a flat flame burner matrix configuration (as described in detail in [20]) consisting of a central burner (20 mm diameter), a rind-shaped co-annular burner (56 mm outer diameter), and another ring-shaped co-flow (86 mm outer diameter), separated by 1 mm thick rings. Shown are mole fraction radial profiles at three HAB.

Enclosed burners additionally encounter the effect of heat transfer between the flame and chamber walls and modified fluid flow, guiding of flame gases towards the exhaust opening [22]. These combined effects lead to velocity, temperature, and species concentration variations across the burner and therefore can affect the conditions along the center line, which complicates comparisons between experiments and simulations – especially when obtained in different burners. Furthermore, the resulting variations need to be considered when interpreting data obtained from line-of-sight integrated measurement techniques.

The differences found in previous measurements of the soot volume fraction (f_V) in various premixed flat flames from different labs, as presented in Figure 2, triggered the investigation presented in this paper. Both, burners that are open to the atmosphere (OB) and enclosed burners (EB) are considered here. Premixed open ethylene/air flames of $\phi = 2.1$ and 2.34 with matrix diameters of 48 and 60 mm shielded by a nitrogen coflow were studied at atmospheric pressure by Carbone et al. [23] and Xu et al. [24], respectively. In our lab, f_V was measured by Mi et al. [21] using three-pass extinction in an enclosed 20-mm diameter burner shielded by a non-sooting methane flame of $\phi = 1.2$. The same burner was investigated in this work without enclosure by cavity ring-down extinction (CRDE) [5, 25, 26]; this was necessary because any additional optical losses in the beam path between the high-reflectivity mirrors by, e.g., optical

windows, will severely reduce the detection sensitivity in this method and make soot detection in the ppb concentration level impossible. In some measurements, the matrix diameter was extended to 56 mm by operating the central circular disk and the surrounding matrix ring (previously used for operating a shielding non-sooting methane flame of $\phi = 1.2$; note that both zones are separated by a 1-mm-wide stainless steel ring [20]) with the same gas mixture. In this case, a third ring-shaped matrix is providing an outer shielding coflow of nitrogen. The full description to the experiment is presented in the supplemental material.

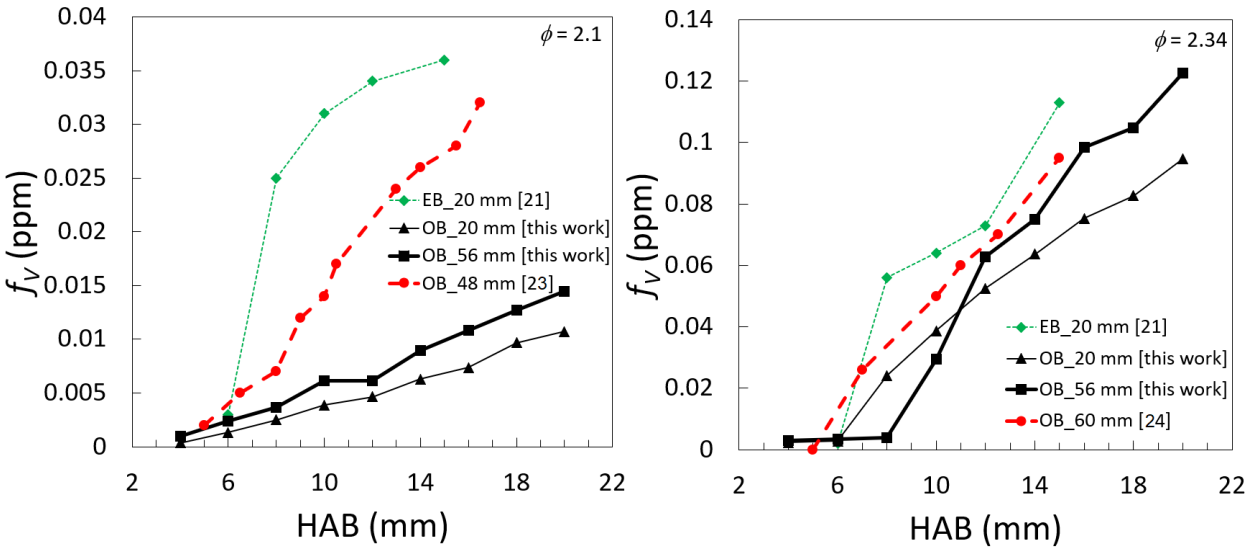

Figure 2: Measured soot volume fractions f_V in enclosed (EB) and open (OB) burners operated with premixed ethylene/air flames of ϕ = 2.1 and ϕ = 2.34 at atmospheric pressure. Various diameters of burner matrices were used as given in the legend. Diamonds: Three-pass extinction data [21], circles: Laser extinction data for ϕ = 2.1 [23] and ϕ = 2.34 [24], triangles and squares: Cavity ring-down extinction data (this work).

As can be seen in Fig. 2, for the ϕ = 2.34 sooting flame, the experimental data are in relatively good agreement (within a factor of about two). The results diverge more strongly for the low-sooting flame at ϕ = 2.1, where the enclosed burner shows higher f_V than those of Carbone et al. [23] even with a 20 mm matrix diameter, while the larger diameter open burner f_V results are closer (although still far off) to those of Carbone et al. [23]. All these variations of experimental data on one physical quantity (f_V) in dependence on the burner configuration makes data inter-comparison difficult, especially for soot formation at near-threshold conditions (i.e., ϕ = 2.1), where small changes in oxygen concentration that can be caused by diffusion would alter soot formation/oxidation rates.

For maintaining 1D flow conditions, burners of infinitely large diameter would be ideal for providing a central flame zone undisturbed by the environment. In such a case, axial profiles of combustion species and temperature would depend only on the operating conditions, such as inlet velocity, fresh-gas composition, temperature and pressure. In practice, therefore, burners with a sufficiently large matrix diameter would be

preferred, as long as the gas inlet-velocity and the temperature homogeneity of such matrices can be ensured. Therefore, this work presents an experimental investigation of the correlated influence of the diameter and of shielding coflows in premixed sooting flames caused by lateral diffusion of species and heat. Furthermore, as there is still no chemistry mechanism that can accurately predict soot-formation at the specific near-threshold conditions of this work, we compare the experimental findings to simulations based on established soot-formation mechanisms to find the best compromise for experiment design. This concerns the range of matrix diameters (up to 60 mm) and the effect of different types of outer shielding flows using either inert gases or reactive flows, which are able to produce almost unchanged temperature and species profiles independent of the burner configuration. To this end, the following strategy is applied:

I. We benchmark our modeling approach against experimental data for methane/air flames of Do et al. [3] and ethylene/air flames of Carbone et al. [23] at near-threshold sooting conditions.
II. We systematically study 2D simulations for each target burner configuration (diameters: 20, 40, and 60 mm; inert and flame shielding). The simulation results are then analyzed to indicate appropriate burner configurations for achieving quasi unaffected axial temperature and species profiles.
III. As an experimental demonstration, we compare trends of simulated axial soot volume fraction with experimental data for selected burner configurations.

2. Simulation conditions and approaches

Several recent studies focused on soot formation at near-threshold sooting conditions, e.g., of Desgroux et al. [6, 7, 25, 27-31] and Gleason et al. [6, 25, 27, 32, 33]. Two cases, premixed ethylene/air and methane/air flames were selected for the present investigation. The first one is a target flame for soot studies listed at the International Sooting Flame Workshop (ISFW) [34] as an atmospheric laminar premixed low-sooting ethylene/air flame $\phi = 1.2$ [23], which was the subject of several modeling and experimental investigations [14, 17, 21, 23, 35-38]. The second one is an atmospheric pressure laminar premixed methane/air flame operated at the threshold of soot formation of $\phi = 1.82$ [3]. Table 1 presents the main operating conditions of the selected flames for this investigation.

2D simulations are accomplished by assuming burner plates of increasing diameters, i.e., adding annular rings with a width 10 mm to cover the target flame diameter of 20 mm and increasing their diameters to 40 and 60 mm, respectively. Each such burner matrix is surrounded by an additional concentric ring for the shielding coflow consisting of either nitrogen or another flame. In a practical experiment, such combined concentric matrices are separated by a narrow metal ring and the resulting discontinuity in flow conditions can have a significant effect on local temperature, species concentrations and soot formation. In 2D

simulations, this effect is found to have a limited effect on these global quantities, therefore, we consider here an idealized case of directly interconnected co-annual matrices. Figure 3 shows the computational domain applied in Fluent®, where a 2D axisymmetric laminar flow simulation on a uniform mesh has been employed containing ~8000 cells, adequate to ensure grid-insensitive results of reactive flow over the four burner matrices and therefore not focus solely on axial parameter changes or near critical regions like the stagnation plate, which is not crucial for this work. In the simulations, the P1 radiation model [39] was adopted to approximate gas-phase thermal radiation, and soot formation was simulated using the Moss-Brookes soot formation model [40], while the CHEMKIN-CFD solver of Appel el al. [41] and GRI-3.0 [42] mechanisms for ethylene/air and methane/air combustion are implemented, respectively. Two soot formation models are available in Fluent because of their limited computational cost. Both the semi-empirical two-equation Moss-Brookes model considering acetylene and ethylene as soot precursors [40] and the Frenklach method of moments [43] were tested. The Moss-Brookes model was then adopted for its better prediction of the flame conditions investigated in this work. The inlet temperature of the unburnt gas is set to 323 K [14, 23] and boundary conditions are air at standard temperature and pressure. Simulations were carried out for the two flames described in Table 1. The target flame (TF) was surrounded either by a non-sooting methane/air (ϕ = 1.2, v_g = 6 cm/s) co-annular flame (CF) or by a N_2 coflow (CN) at v_g = 21 cm/s. Table 2 shows the combinations that were investigated in the simulations. N and M indicate cases with surrounding nitrogen coflow or flame, respectively, and the numbers (20–60) indicate the diameter of the target flame matrix in mm. All cases given in tables 1 and 2 were studied for 1 and 10 bar.

Table 1: Main operating conditions of the studied flames. Inflow velocities are identical for the 1 and 10 bar simulations.

Fuel	C/O ratio	ϕ	Stagnation plate distance and temperature (mm, K)	Fuel/air inlet velocity v_g / (cm/s)	N_2 coflow inlet velocity v_g / (cm/s)	Burner diameter / mm	Ref.
C_2H_4	0.69	2.1	40, 900	5.87	21	48	[23]
CH_4	0.45	1.82	22, 700	8.79	22	60	[3]

Table 2: Burner configurations considered in the 2D simulations. See text for labeling of the flame/burner configurations.

Case/Matrix inlet	**1**	**2**	**3**	**4**
N20	TF	CN	-	-
N40		TF	CN	
N60			TF	CN
M20		CF	-	-
M40		TF	CF	
M60			TF	CF

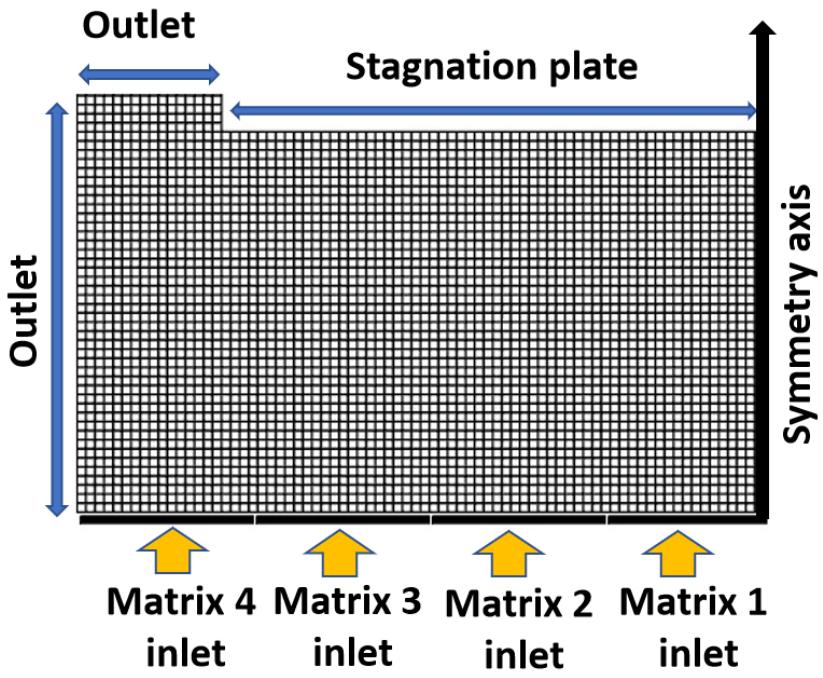

Figure 3. Mesh and boundary conditions used in the 2D simulations.

3. Results and discussion

3.1. Simulation capability for near-threshold sooting flames

To ensure that our simulation approach is able to appropriately predict soot formation, we use the semi-detailed mechanism of Appel el al. [41] and in a first step compare the simulation results with experimental data for premixed ethylene/air flames (ϕ = 2.1) from Carbone et al. [23]. The data contains species concentrations from gas chromatography coupled with mass spectrometry (GC/MS), temperature from either thermocouple or soot pyrometry measurements, and soot volume fractions from light extinction measurements. The flame (cf. Table 1) was stabilized with a 150-mm diameter stagnation plate 40 mm above a 48-mm diameter stainless-steel honeycomb burner matrix and shielded by a N_2 coflow emanating from a co-annular matrix with an outer diameter of 76 mm. The stagnation plate reached a steady-state temperature of 900±50 K. The second data set is from a premixed methane/oxygen/nitrogen flame (ϕ = 1.82) stabilized by a stagnation plate 22 mm above the matrix of a 60-mm diameter McKenna burner by Do et al. [3, 29] (cf. Table 1). Since the aim of this work is not the numerical prediction of experimental data of the studied flames, these comparisons are moved to the Supplemental Material. Figures S2–5 show that for both the ethylene and methane low-sooting flames, the simulation is in reasonable agreement, at least as far as the trend is concerned, with the measured centerline profiles of temperature and major species concentrations, especially the target one of f_V, as shown in figure 4 extracted from figures S3 and S5, which makes it possible to consider their results in this study as a compass indicator for perspective investigations.

CO and H_2 concentration profiles were chosen for comparison due to their importance in soot formation [44-47] and those considered as soot precursors of C_4H_4, C_2H_2, C_6H_6, and naphthalene [48].

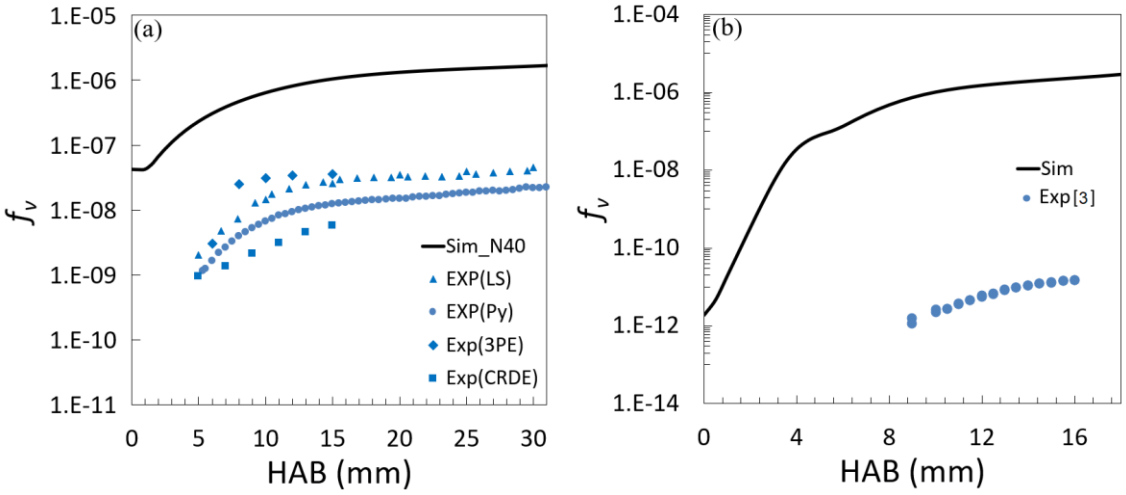

Figure 4. Experimental data (Symbols) and simulated (lines) axial profiles of f_V vs HAB of ϕ = 2.1 C_2H_4/air atmospheric pressure premixed flame (a) [21, 23] and ϕ = 1.82 $CH_4/N_2/O_2$ atmospheric premixed flame (b) [3].

3.2. **Simulation-based investigation of the influence of the burner configuration**

To investigate the effect of the matrix diameter variation and the type of shielding flow on soot formation, the flame conditions presented in table 1 are investigated based on simulations for all the burner configurations listed in table 2 using the approaches described in sections 2 and 3.1. Axial temperature, f_V and CO, H_2, O_2, C_2H_2 concentration profiles predicted by 2D simulation are selected to be compared for the different burner configurations and both near-threshold sooting flames of Carbone et al. [23] and Do et al. [3, 29]. Figure 5 shows a comparison between the axial profiles of temperature, CO, H_2, O_2, and C_2H_2 concentration, and f_V as a function of HAB and for the different burner configurations described in table 2 of the premixed ϕ = 2.1 C_2H_4/air flame at atmospheric pressure (thin lines) and at 10 bar (thick lines). The burner configurations affect the species concentration profiles in different ways (Fig. 5a–d). These differences originate from the difference in flame temperature (Fig. 5f) caused by, e.g., the variation in local oxygen concentration (Fig. 5d) due to oxygen diffusion and potential additional effects of lateral heat transfer. The difference in the axial profiles is more important for atmospheric flames and at larger HABs. As the diameter of the studied flame increases, this difference becomes small and the axial profiles of gas temperature and species approach those of a quasi-flat flame. This is true for both shielding flows (N_2 or surrounding flame) of the target flame. It is important to note that the temperature profiles significantly differ between the two kinds of target flame shielding, with the most prominent effect on the small-diameter target flames. In addition, flame shielding provided higher soot production than nitrogen shielding by reducing the temperature variation towards the edges.

A flame with a relatively large matrix diameter would provide much less disturbed axial profiles of combustion products and temperature, and could therefore be simulated as a one-dimensional flame. In this respect, a relative percentage error, defined as $100(T_{N60}–T_{N80})/T_{N80}$, is calculated of the axial temperatures at 1 and 10 bar along all the studied HABs for a supplemental case of a burner with a 80-mm matrix diameter (N80). These two case studies use N_2 shielding. The predicted deviation does not exceed 0.65 % in temperature, i.e., below 12 K. Therefore, we can deduct for the studied flame conditions in Table 2 that the 60-mm diameter N_2-shielded burner approximates the ideal case of an undisturbed target flame.

The influence of lateral species and heat transport on the soot volume fraction is especially significant at atmospheric pressure and for near-threshold conditions. Therefore, only the atmospheric near-threshold sooting $CH_4/O_2/N_2$ flame configuration of $\phi = 1.82$ is studied here. The temperature profiles predicted by 2D simulations as function of HAB presented in Fig. 6a differ in their relative position for flames N20, N40, and M20, and almost fall on top of each other for the other flames (M40, M60, and N60, named 'rest'). Therefore, the axial profiles of f_V, O_2, C_2H_2, CO, and H_2, as key indicators of soot formation, for N20, N40, M20, and 'rest', are presented for comparison in Figure 6b–f, respectively.

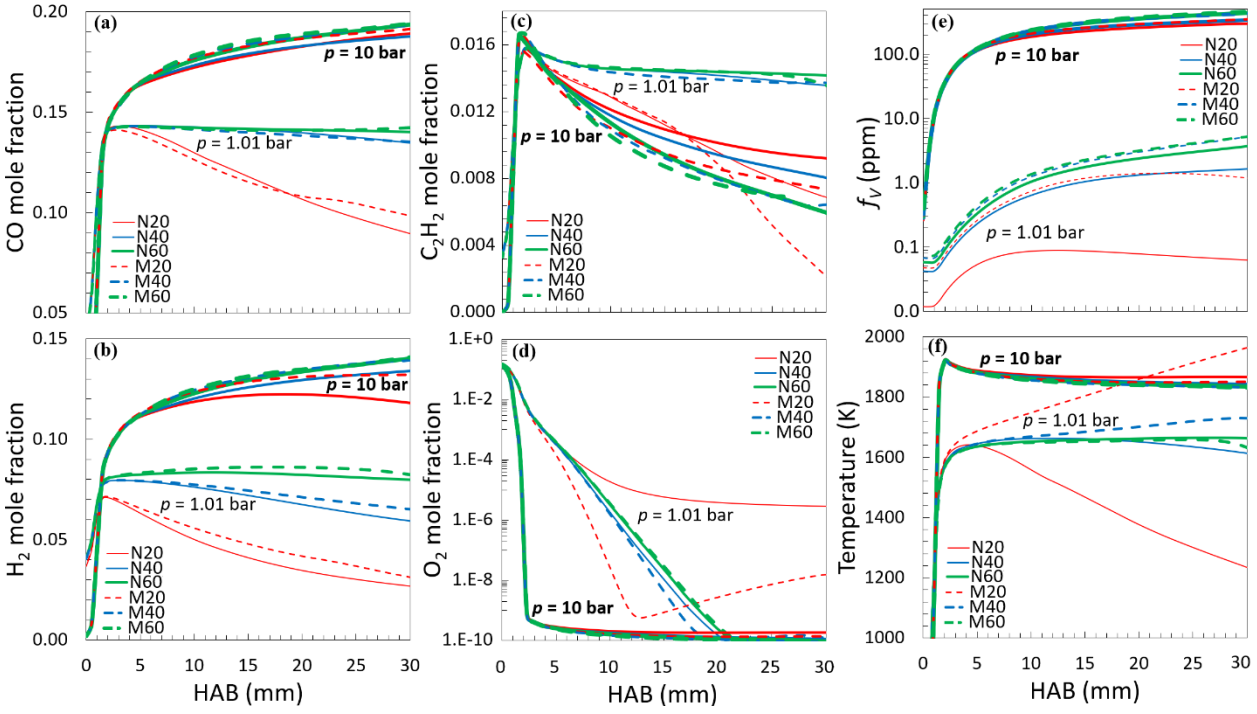

Figure 5. Predicted axial profiles of species mole fraction a: CO, b: H_2, c: C_2H_2, d: O_2, e: f_V and f: Temperature vs. HAB for $\phi = 2.1$ C_2H_4/air premixed flame at atmospheric pressure (narrow lines) and 10 bar (bold lines). Shielding coflow is N_2 (solid lines labeled N and the diameter of the flame in mm) or non-sooting methane flame (dotted lines labeled M and the diameter of the flame in mm).

The significant difference in the temperature profiles of N20, N40, M20, and 'rest' flames, shown in Fig 6a, demonstrates the influence of the nature of the coflow on the combustion temperature of the target flame, which in turn affects the species profiles as also seen for the axial profiles of f_V, O_2, C_2H_2, CO, and H_2 (Fig. 6b–f). An earlier temperature increase results in an earlier rise in product species formation. The further development of the species concentration profiles afterwards depends on the thermochemistry and the influence of the environment through lateral diffusion. The relatively high temperature and the earlier temperature rise of flame M20 promotes the formation of CO and H_2 and the consumption of O_2, however, it does not positively affect soot formation as also seen for the delayed rise in the N20 flame. The high (more than 1800 K) plateau temperature of the M20 flame inhibits soot formation by enhancing oxidation. The maximum soot production is decreasing with flame configuration in the order of 'Rest', N40, N20, and M20. Therefore, it can be concluded that it would be necessary for the appropriate evaluation of soot for a near-threshold methane/air premixed flame to have an inner burner matrix of at least 40 mm diameter shielded by a methane non-sooting flame (i.e., the "M40-flame"), or a 60 mm inner matrix diameter shielded by a N_2 coflow (i.e., the "N60-flame"), or a non-sooting methane/air flame (i.e., the "M60-flame") – named 'rest' in Fig. 6 (cf. table 2).

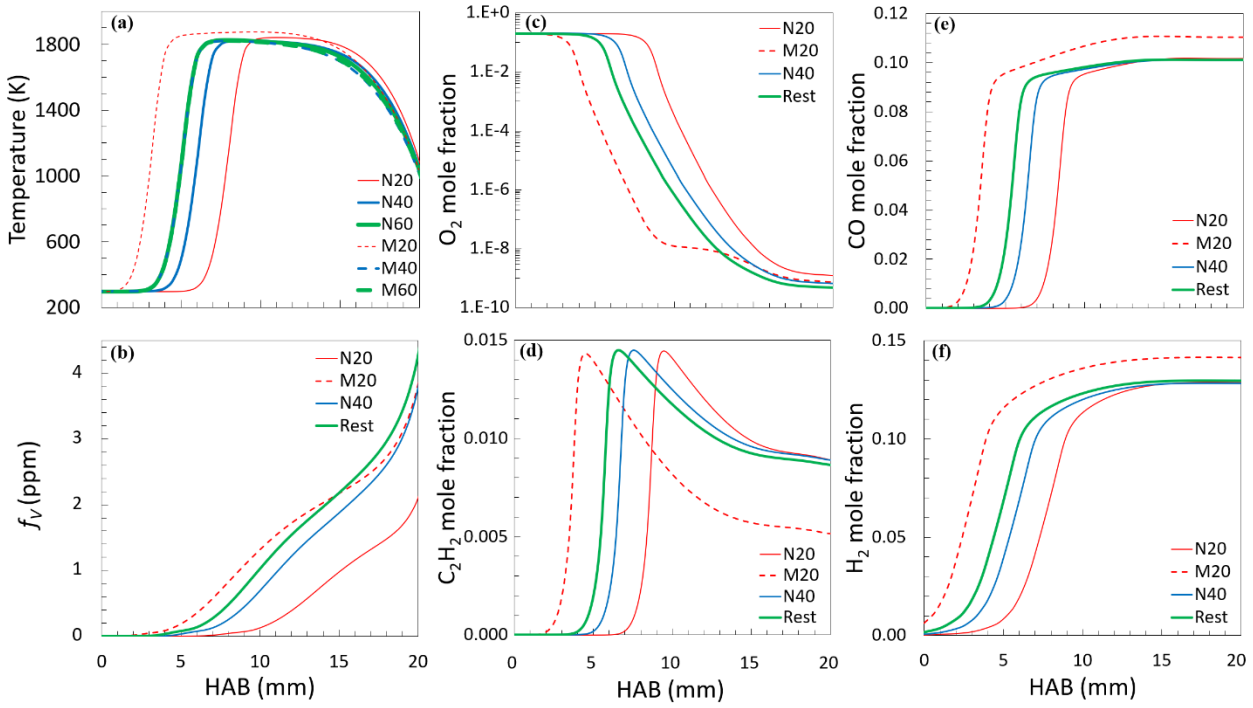

Figure 6. Predicted axial profiles of a: temperature, b: f_V, and species mole fraction c: O_2, d: C_2H_2, e: CO, f: H_2 vs HAB of ϕ = 1.84 CH_4/air atmospheric premixed flame. 'Rest' represents the quasi-superimposed profiles of M40, M60, and N60 flames, cf. table 2.

3.3. **Experimental demonstration**

The simulation-based evaluation shown above is now compared to measurements for the N20, M20, and N60 burner configuration (cf., table 2) operated with an ethylene/air mixture with $\phi = 2.1$ at 1 bar. The soot volume fraction f_V was measured with cavity-ringdown extinction (CRDE) with pulsed 1064-nm radiation following the approach described by Betrancourt et al. [26]. Figure 7 shows color-camera photos and false-color maps of 2D simulations of temperature, C_2H_2 mole fraction, and f_V for the three flame configurations (columns). In the case of a nitrogen coflow (N20, N60), the larger flame diameter leads to a broader soot-containing zone and higher f_V indicating the strong influence of the environment on the N20 flame. When changing the coflow from nitrogen to a flame (N20 vs. M20), the soot-loaded zone gets wider and f_V increases, indicating that the surrounding flames provides improved but not perfect shielding against the environment. These effects correlate with the variations in temperature (Fig. 7b).

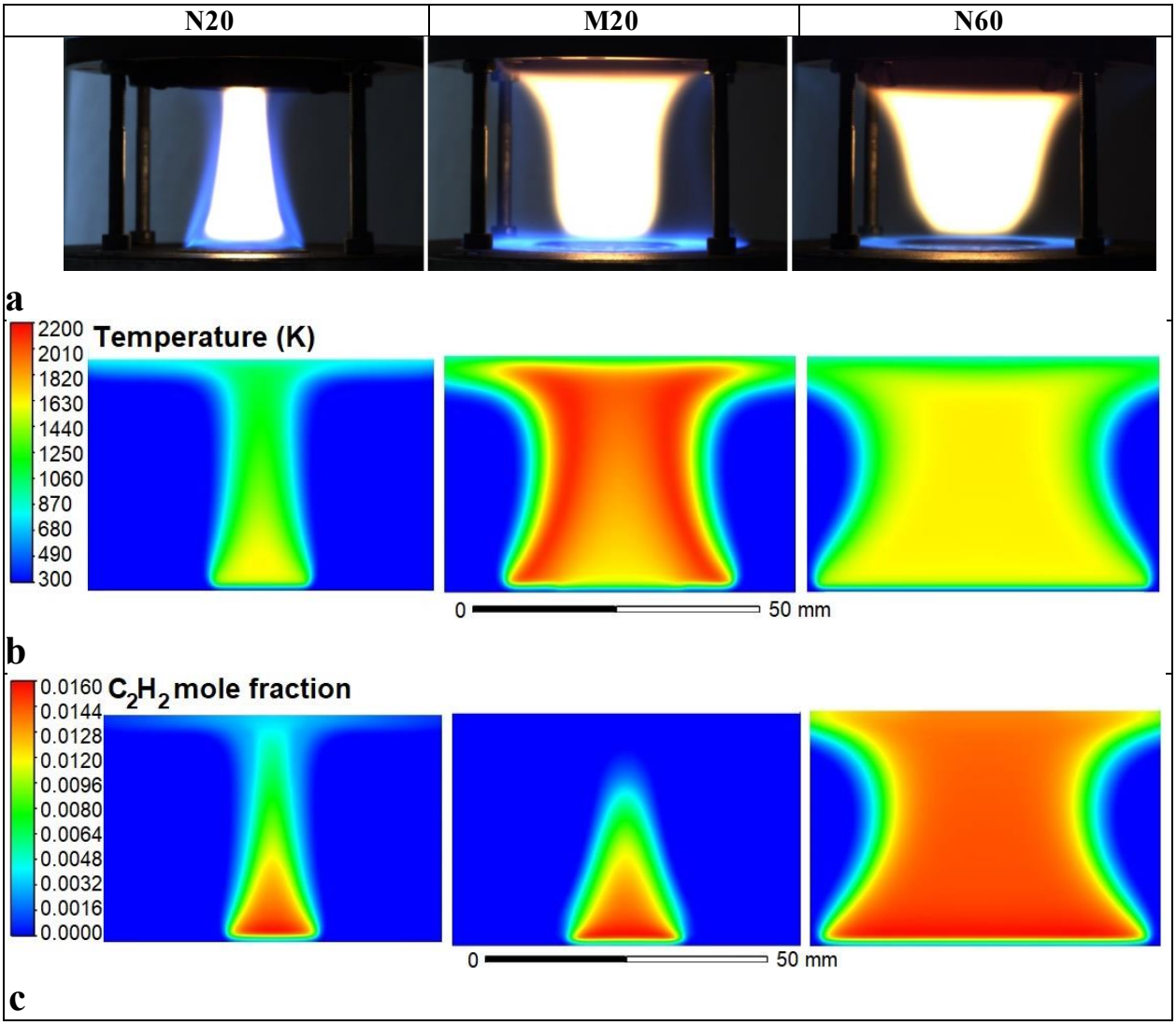

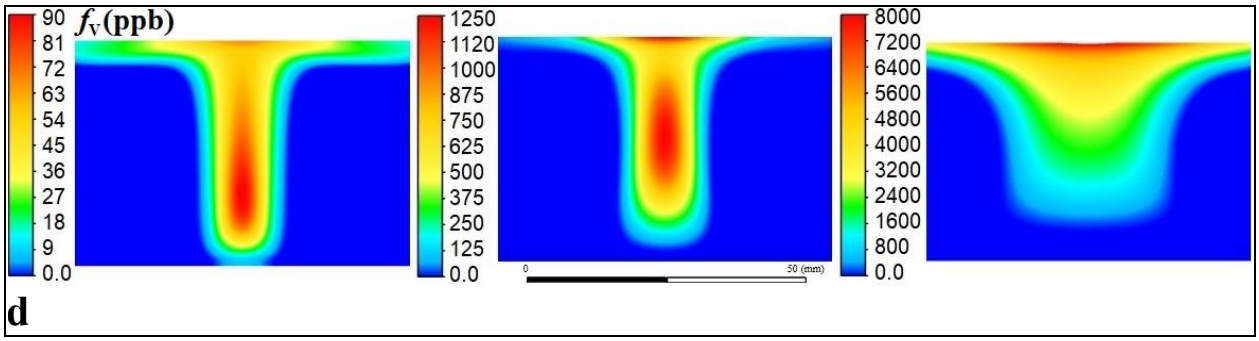

Figure 7. Flame photos (row a) and temperature (row b), acetylene mole fraction (row c) and f_V (row d) from 2D simulation in false-color plots of the atmospheric ethylene/air target flame of ϕ = 2.1, cf. Table 1, using the burner configurations M20, N20, and N60 given in Table 2.

Figure 8a presents the variation of the temperature and gas velocity profile evolution along the centerline with HAB for the three studied flames retrieved from the 2D simulations. The post-flame gas temperature generated in the M20 flame exceeds 1800 K, which does not favor higher soot production than in the N60 flame. The corresponding temperature rise to about 1700 K provided by the N60 flame favors the highest production of acetylene and soot. The N20 flame shows the lowest temperature, acetylene concentration, and thus soot f_V, which can be attributed to the more dominant lateral transport effects of this burner configuration. In this flame, the zone with high gas temperature and f_V narrows close to the stagnation plate (left column in Fig. 7), where the axial gas velocities are maximal as shown in Fig. 8a. This zone is located below the stagnation plate at HAB = 24 mm, where the diffusion of particles, flame stretch, and radial velocity are maximal [14].

The influence of lateral species diffusion and heat transfer manifests itself through significant differences in the axial temperature profiles of the M20, N20, and N60 flames in Fig. 8a. This observation raises the question whether the effect is dominated by species diffusion or by heat transfer. The M20, N20, and N60 flames are therefore assumed to be surrounded by either N_2 at 300 K (SN2) to prevent oxygen diffusion, by air with zero heat flux (SAA) to prevent lateral heat transfer, or by N_2 with zero heat flux (SAN) to prevent both oxygen and heat transport from the environment. The respective predicted temperatures (T_n) are labeled with a corresponding index (n = SN2, SAA, or SAN). As reference (named T_{ref}), the case with surrounding air at 300 K shown in Fig. 8a is used. Figure 8b presents a comparison between the predicted relative axial temperature percentage, referred to here as (T_r %) and defined as 100 ($T_n - T_{ref}$)/T_{ref}, as a function of HAB. The shielding of the smallest target flame (20 mm matrix diameter) by the reactive coflow of the non-sooting methane/air flame (M20) shows the strongest disturbance by this lateral influence of oxygen diffusion and heat transfer. At HABs below 16 mm, the order of decreasing T_r% is given by the SAN, SAA, and SN2 surrounding and switches to SAN, SN2, and SAA for higher HABs, respectively. A consistent and modest T_r% difference between the SAN and SN2 cases along all HABs with a more

significant one between the SN2 and the reference air surrounding case at 300 K is observed. The latter indicates that for the 20-mm diameter flame, the lateral effect of oxygen diffusion is more important than that of heat transfer at all HABs. This smallest target flame diameter of 20 mm shielded by a N_2 (N20 flame) demonstrates much less disturbance than the high-temperature coflow of the non-sooting flame shielding (M20 flame), with conserving almost the same trend in the variation in disturbance of SAN, SAA, and the SN2 surrounding. The deviation from the reference surrounding case is higher for SAN than for SAA only for high HABs > 15 mm, where the shielding effect of the inert shielding coflow becomes weak. The difference in disturbance of the on-axis conditions between the SAN and SN2 surroundings is significant and increases as a function of HAB with a slight increase for SN2 compared to SAN regarding the reference surrounding case along HAB. This shows that the effect of oxygen diffusion is slightly greater than that of heat transfer at all HAB positions. The smallest perturbation is observed for the target flame of 60 mm diameter shielded by N_2 coflow (N60), where the SN2 case shows almost no perturbation due to the effect of oxygen diffusion from the surrounding. As the T_r% profiles of SAN and SAA surroundings are almost superimposed and show a modest perturbation compared to the reference case along all HABs, it can be concluded that for the 60-mm diameter flame, the heat transfer has a dominant effect compared to that of oxygen diffusion at all HAB.

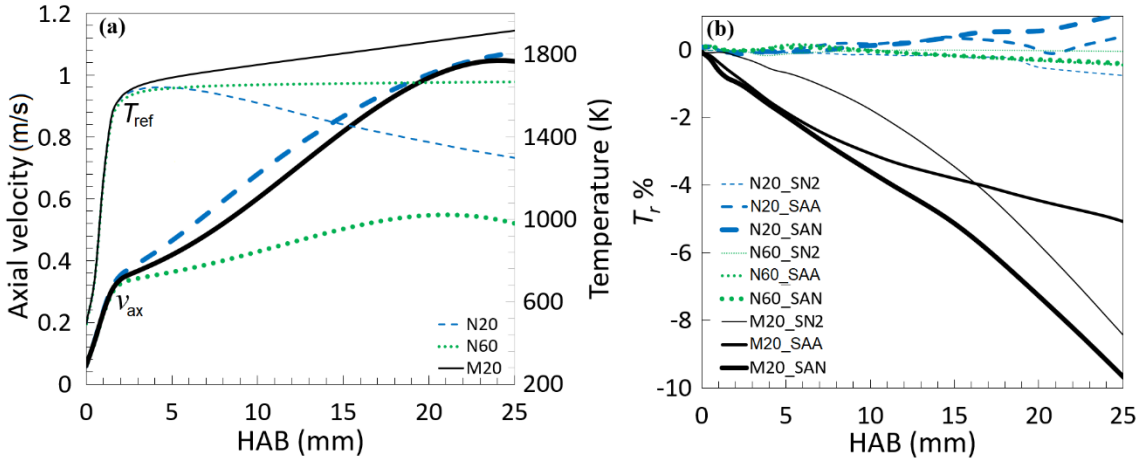

Figure 8: (a) Variation of axial temperature (T_{ref}) and gas velocity (v_{ax}) vs. HAB for the ϕ = 2.1 C_2H_4/air atmospheric pressure premixed flame for the M20, N20, and N60 burner configuration, cf. Table 2. (b) Change of T_r%; 100 (T_n – T_{ref})/T_{ref}, vs. HAB for M20, N20, and N60 flames of axial temperature T_n surrounded by either N_2 at 300 K (SN2), air without heat transfer (adiabatic) (SAA) or N_2 without heat transfer (SAN) surrounding. T_{ref} is the reference case temperature of the same flames in an air surrounding at 300 K.

The 2D simulations in false-color plots of temperature, species and soot concentrations presented in Fig. 7 visualize the influence of lateral species and heat transport for the M20, N20, and N60 configurations. To further illustrate these scenarios, Figure 9 presents radial profiles of temperature, f_V, acetylene and oxygen mole fraction at HAB = 10 mm and HAB = 24 mm (around the maximum axial velocities of burned gases)

of the three burner configurations (cf. Figure 8a). Figure 9a shows that the extent of an almost constant temperature level increases significantly from configuration N20 to M20 and N60 for both selected HAB, which is due to the lower influence of lateral transport accompanied with the larger matrix diameter resulting in the higher f_V and the wider sooting zone of N60 and then M20 with respect to N20, as seen in Figs. 7a, 7d and 9c. Nevertheless, the Moss-Brookes model was not able to predict sufficiently well the significant influence of lateral species diffusion and heat transfer at high HABs of the N20 flame, where the experiment, Figs. 7a and 9c, shows a narrow soot zone at the top compared to a broad zone at the bottom. The effect of temperature as well as the more extended zone of unaltered high concentration of acetylene on soot formation visible in Figs. 9a–c is obvious for the N60 burner configuration. In spite of almost the same concentration of acetylene produced in the M20 and N20 flames, the soot production of M20 is significantly higher than that of N20, which relates to the more appropriate (i.e., higher) temperatures for soot formation [8, 9] achieved in M20 compared to N20. However, the wider fields with almost constant temperature and acetylene mole fraction shown in Figs. 7b–c and 9a–b at HAB = 10 mm relative to HAB = 24 mm, where the axial velocities of hot gases are maximal, generates consequently larger sooting zones and higher f_V, as shown in Figures. 7a, 7d, and 9c.

Despite the observed overestimation of the 2D simulation of f_V compared to the experimental data as seen in Figure 9c, the measured radial profiles of f_V (derived from CRDE measurements) show the same trend of decreasing soot production as a function of radial position compared to the simulation results when moving from the N60 and M20 to the N20 flames. The experimental decrease in the width of the sooting zone is also reproduced by the simulation when switching from N60 on M20 to N20 flame. The radial positions of the lateral dips in O_2 mole fraction (x_{O2}) shown in figure 9d visualize the borders of this lateral influence of the surrounding on the target flames. The hot core of the rich target flame first consumes its own oxygen supplied by the inlet of fuel/air mixture representing a specific x_{O2} along the burner centerline for each HAB and burner configuration. A decrease in x_{O2} at a larger distance from the centerline starts when the effects of mixing and diffusion from the surrounding become significant. This affects the combustion rate of fuel/air mixture of target flame reaching a maximum after which a fast increase in x_{O2} occurs where the lateral oxygen diffusion arises and the amount of fuel decreases in the mixing zone between flame and shielding coflow. For each burner configuration, these positions are closer to the burner centerline for HAB = 24 mm, where this lateral influence is higher than at the low HAB of 10 mm. The dip radial positions are farther from the burner centerline for both HABs following the order N20, M20, and N60 of burner configuration, which is the same order as that already noticed with the width of temperature, acetylene, and soot fields, and also with the acetylene and soot concentration profiles in Figs. 7 and 9.

Figure 10 presents a comparison between the measured (using CRDE diagnostic) and predicted axial f_V profiles obtained from 2D simulations of the $\phi = 2.1$ C_2H_4/air atmospheric pressure premixed flame and for the N20, M20, and N30 configurations. The overestimations of the Moss-Brookes soot formation model [40] implemented in 2D simulations of 89, 1110 and 1620 ppb at HAB = 14 mm, compared to the experimental data are observed as seen also in Fig. 4 and Fig. S3h in the supplemental material, where the predictions of simulation approach are compared. The influence of lateral transport is clearly visible in the measured and the simulated f_V, especially at high HABs where the diffusion of species, flame stretch, and radial velocities are maximal [14]. At these high HABs, the highest f_V is measured for the largest diameter of target flame (N60) to be followed by M20 with an intermediate soot production and finally the lowest one by N20. This shows that the f_V are higher when the non-sooting flame of methane forms the flame shield to the target flame (M20) instead of a room temperature nitrogen flow (N20). This behavior could be explained by the high temperature of the burned gas (Figs. 8a and 9a) generated by the surrounding non-sooting methane/air flame, where heating through the external flame promotes soot formation [8, 49]. The Moss-Brookes soot formation model [40] implemented in the 2D simulation predicts well this decrease in f_V, shown also in figures 7d and 9c for the N60, M20, and N20 configurations. Accordingly, these results demonstrate the influence of the burner diameter and the nature of the shielding coflow on f_V. Moreover, it is important to note that the simulation was not able to well predict the reduction in f_V at HAB > 14 mm of the N20 flame (Fig. 10), which is attributed to the increased influence in lateral transport at high HAB. These observations require further experimental and modeling investigations.

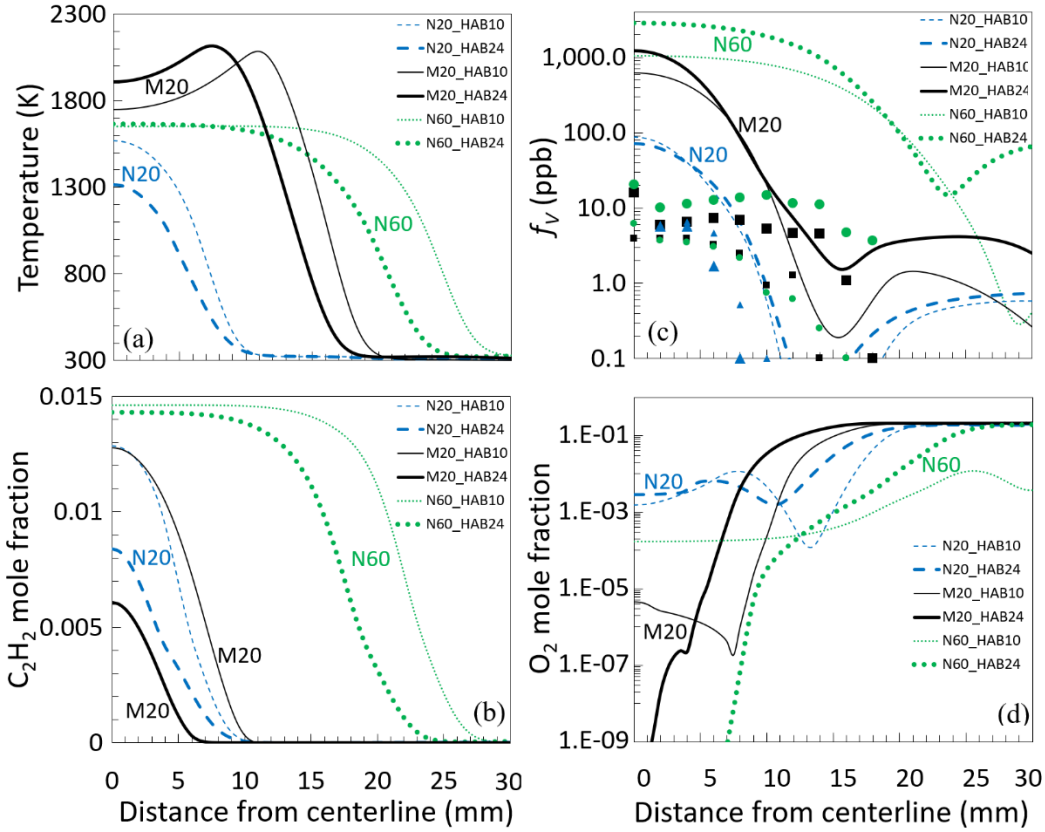

Figure 9: Radial profiles of temperature (a), acetylene mole fraction (b), f_V (c), and oxygen mole fraction (d) for the M20, N20, and N30 burner configurations, cf. Table 2, of the ϕ = 2.1 C_2H_4/air atmospheric pressure premixed flame at HAB = 10 mm (thin lines for simulation and small symbols for experiment) and 24 mm (thick lines for simulation and big symbols for experiment). Circles, squares, and triangles represent the f_V CRDE experimental results of N60, M20, and N20, respectively.

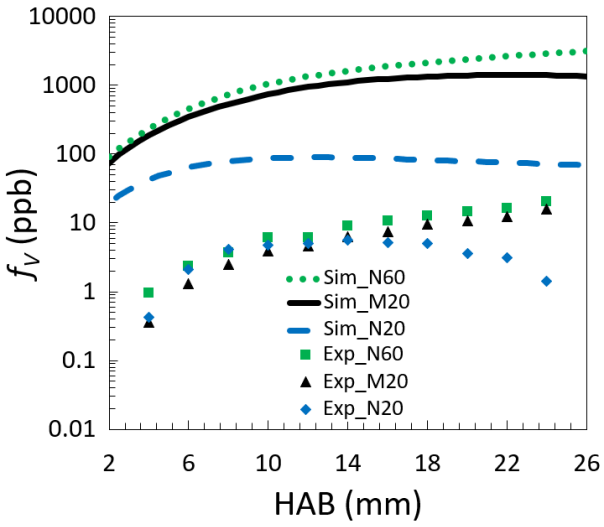

Figure 10. Experimental (symbols) and simulated (lines) axial profiles of f_V vs. HAB of ϕ = 2.1 C_2H_4/air atmospheric pressure premixed flame, cf. Table 1, and for the M20, N20, and N60 configurations, cf. Table 2.

4. Conclusions

The combined influence of the premixed flame diameter and shielding coflows, and consequently that of lateral species diffusion and heat transfer was investigated experimentally by measuring f_V of atmospheric premixed ethylene/air flames ϕ = 2.1 and 2.34 using cavity ring-down extinction (CRDE) measurements. As the underlying motivation is to provide the best suitable experimental data for analyzing soot formation at near-threshold sooting conditions, laminar premixed ethylene/air (ϕ = 2.1) and methane/O_2/N_2 (ϕ = 1.82) flames stabilized with stagnation plates at 40 and 22 mm above the burner, respectively, are simulated for comparison. 2D simulations were conducted using Fluent implementing the semi-detailed mechanisms of Appel el al. [41] and GRI-3.0 [42]. Flame diameters of 20, 40, and 60 mm shielded by either a nitrogen coflow or a non-sooting methane/air flame were considered operating at atmospheric pressure and 10 bar. The simulated temperature and species profiles resulting from the simulations were compared to experimental data from the literature [3, 21, 23] (see Supplemental Material) and new soot volume fraction measurements.

At 10 bar, the low-sooting ethylene/air flames stabilized on burners with 20- and 40-mm diameters show significant divergence from those with 60-mm diameter in the species profiles along the centerline, especially for hydrogen and acetylene concentrations at HAB > 10 mm. This divergence is modest at all HAB for temperature, CO concentration, and soot volume fraction f_V with less than 2, 5, and 5 % deviation, respectively.

The burners with 20- and 40-mm diameter operated under atmospheric pressure with ethylene and methane show more significant influence of the flame environment on temperature, species concentration, and f_V compared to those with 60-mm diameter. For the low-sooting ethylene/air flame (ϕ = 2.1), the CO and acetylene concentration and the soot volume fraction profiles were almost unaffected by changes in the flame environment for burner diameters starting from 40 mm. The atmospheric pressure flame configurations of Do et al. [3] operated at near-threshold sooting condition (ϕ = 1.82) show also quasi unchanged profiles of temperature, species concentrations and f_V for a flame diameter from 40 mm and larger using the methane non-sooting flame as a shielding coflow, or for a burner diameter of 60 mm for whatever is the used as shielding flow.

The soot volume fraction as a function of HAB of the atmospheric ethylene/air flame (ϕ = 2.1) of 20-mm diameter flames applying the two kinds of shielding coflow (N_2 and CH_4/air flame) and of 60-mm diameter flames with only N_2 shielding were measured by cavity ring-down extinction (CRDE). The results were compared to results from 2D simulations. The difference between measured and simulated f_V profiles with

burner diameter and kind of shielding emphasizes the impact of lateral species and heat transport on the soot formation in the flames. The simulations show that the influence of lateral transport on the temperature of the 60-mm diameter flame is mainly due to heat transfer with almost negligible influence of oxygen diffusion. At 20-mm flame diameter, the influence is reversed and oxygen diffusion becomes the main influential factor.

The inhibiting roles of temperatures above 1800 K on soot formation [50], and the promoting one at $T \approx 1700$ K are observed. Experimental and 2D simulation results of different ethylene/air flame configurations show that the width of the formed soot zone follows the width of the almost unchanged radial profiles of temperature and acetylene concentration. The high axial gas velocities and the influence of lateral species and heat transport located far away from the burner matrix and below the stagnation plate, affect the rise of temperature and acetylene concentration and consequently soot formation.

Acknowledgments

Financial support by the German Research Foundation (DFG) within the project "Soot nucleation in low-sooting high-pressure flames: Experiment and modeling" (No. 439059510) is gratefully acknowledged. The authors thank Thomas Dreier (EMPI, University of Duisburg-Essen, Germany) and Pascale Desgroux and Nathalie Lamoureux (PC2A Laboratory, University of Lille, France) for their important assistance in this work.

References

[1] F. Migliorini, S. De Iuliis, F. Cignoli, G. Zizak, How “flat” is the rich premixed flame produced by your McKenna burner?, Combust. Flame 153 (2008) 384-393.

[2] S. Chander, A. Ray. Investigation of Effect of Burner Diameter on Heat Transfer Characteristics of Methane/Air Flame Impinging on a Flat Surface. In: ASME 2005 Summer Heat Transfer Conference collocated with the ASME 2005 Pacific Rim Technical Conference and Exhibition on Integration and Packaging of MEMS, NEMS, and Electronic Systems; 2005. p. 213-220.

[3] H.-Q. Do, L.-S. Tran, L. Gasnot, X. Mercier, A. El Bakali, Experimental study of the influence of hydrogen as a fuel additive on the formation of soot precursors and particles in atmospheric laminar premixed flames of methane, Fuel 287 (2021) 119517.

[4] H. Bladh, N.-E. Olofsson, T. Mouton, J. Simonsson, X. Mercier, A. Faccinetto, P.-E. Bengtsson, P. Desgroux, Probing the smallest soot particles in low-sooting premixed flames using laser-induced incandescence, Proc. Combust. Inst. 35 (2015) 1843-1850.

[5] P. Desgroux, X. Mercier, B. Lefort, R. Lemaire, E. Therssen, J.F. Pauwels, Soot volume fraction measurement in low-pressure methane flames by combining laser-induced incandescence and cavity ring-down spectroscopy: Effect of pressure on soot formation, Combust. Flame 155 (2008) 289-301.

[6] T. Mouton, X. Mercier, M. Wartel, N. Lamoureux, P. Desgroux, Laser-induced incandescence technique to identify soot nucleation and very small particles in low-pressure methane flames, Appl. Phys. B 112 (2013) 369-379.

[7] D. Aubagnac-Karkar, A. El Bakali, P. Desgroux, Soot particles inception and PAH condensation modelling applied in a soot model utilizing a sectional method, Combust. Flame 189 (2018) 190-206.

[8] A. Ciajolo, A. D'Anna, R. Barbella, A. Tregrossi, A. Violi, The effect of temperature on soot inception in premixed ethylene flames, Symposium (International) on Combustion 26 (1996) 2327-2333.

[9] K. Ishii, N. Ohashi, A. Teraji, M. Kubo. Soot formation in hydrocarbon pyrolysis behind reflected shock waves. In: editor^editors. Proc. 22nd Int. Colloquium on the Dynamics of Explosions and Reactive Systems; 2009. p.

[10] G. Prado, J. Lahaye, Physical Aspects of Nucleation and Growth of Soot Particles, in: D.C. Siegla, G.W. Smith (Eds.), Particulate Carbon: Formation During Combustion, Springer US, Boston, MA, 1981, pp. 143-175.

[11] R. Whitesides, M. Frenklach, Detailed Kinetic Monte Carlo Simulations of Graphene-Edge Growth, The Journal of Physical Chemistry A 114 (2010) 689-703.

[12] P. Fortugno, S. Musikhin, X. Shi, H. Wang, H. Wiggers, C. Schulz, Synthesis of freestanding few-layer graphene in microwave plasma: the role of oxygen, Carbon 186 (2021) 560-573.

[13] T. Heidermann, H. Jander, H. Gg. Wagner, Soot particles in premixed C2H4–air-flames at high pressures (P=30–70 bar), Phys. Chem. Chem. Phys. 1 (1999) 3497-3502.

[14] W. Pejpichestakul, A. Cuoci, A. Frassoldati, M. Pelucchi, A. Parente, T. Faravelli, Buoyancy effect in sooting laminar premixed ethylene flame, Combust. Flame 205 (2019) 135-146.

[15] C. Kim, F. Xu, P. Sunderland, A. El-Leathy, G. Faeth. Soot formation and oxidation in laminar flames. In: editor^editors. 44th AIAA Aerospace Sciences Meeting and Exhibit; 2006. p. 1508.

[16] M. Hofmann, W.G. Bessler, C. Schulz, H. Jander, Laser-induced incandescence for soot diagnostics at high pressures, Appl. Optics 42 (2003) 2052-2062.

[17] M. Hofmann, H. Kronemayer, B. Kock, H. Jander, C. Schulz, Laser-induced incandescence and multi-line NO-LIF thermometry for soot diagnostics at high pressures, In European Combustion Meeting, Louvain-la-Neuve, Belgium2005.

[18] M.S. Tsurikov, K.P. Geigle, V. KrÜGer, Y. Schneider-KÜHnle, W. Stricker, R. LÜCkerath, R. Hadef, M. Aigner, Laser-based investigation of soot formation in laminar premixed flames at atmospheric and elevated pressures, Combust. Sci. Technol. 177 (2005) 1835-1862.

[19] M. Leschowski, T. Dreier, C. Schulz, An automated thermophoretic soot sampling device for laboratory-scale high-pressure flames, Rev. Sci. Instrum. 85 (2014) 045103.

[20] M. Leschowski, T. Dreier, C. Schulz, A Standard Burner for High Pressure Laminar Premixed Flames: Detailed Soot Diagnostics, Zeitschrift für Physikalische Chemie, 2015, pp. 781-805.

[21] X. Mi, A. Saylam, T. Endres, C. Schulz, T. Dreier, Near-threshold soot formation in premixed flames at elevated pressure, Carbon 181 (2021) 143-154.

[22] O.M. Feroughi, L. Deng, S. Kluge, T. Dreier, H. Wiggers, I. Wlokas, C. Schulz, Experimental and numerical study of a HMDSO-seeded premixed laminar low-pressure flame for SiO2 nanoparticle synthesis, Proc. Combust. Inst. 36 (2017) 1045-1053.

[23] F. Carbone, K. Gleason, A. Gomez, Probing gas-to-particle transition in a moderately sooting atmospheric pressure ethylene/air laminar premixed flame. Part I: gas phase and soot ensemble characterization, Combust. Flame 181 (2017) 315-328.
[24] F. Xu, P.B. Sunderland, G.M. Faeth, Soot formation in laminar premixed ethylene/air flames at atmospheric pressure, Combust. Flame 108 (1997) 471-493.
[25] P. Desgroux, C. Betrancourt, X. Mercier. Development of highly sensitive quantitative measurements of nascent soot particles in flames by coupling cavity-ring-down extinction and laser induced incandescence for improving the understanding of soot nucleation process. In: editor^editors. OSA Technical Digest. In Laser Applications to Chemical, Security and Environmental Analysis; 2018/06/25 2018; Orlando, Florida: Optical Society of America. p. LTu5C.1.
[26] C. Betrancourt, X. Mercier, F. Liu, P. Desgroux, Quantitative measurement of volume fraction profiles of soot of different maturities in premixed flames by extinction-calibrated laser-induced incandescence, Appl. Phys. B 125 (2019) 16.
[27] P. Desgroux, A. Faccinetto, X. Mercier, T. Mouton, D. Aubagnac Karkar, A. El Bakali, Comparative study of the soot formation process in a "nucleation" and a "sooting" low pressure premixed methane flame, Combust. Flame 184 (2017) 153-166.
[28] X.M. T. Mouton, P. Desgroux Evidence of Nucleation Flames: A Valuable Tool for the Study of Soot Particles Inception In 7th European Combustion Meeting, 2015.
[29] A. Mze Ahmed, S. Mancarella, P. Desgroux, L. Gasnot, J.F. Pauwels, A. El Bakali, Experimental and numerical study on rich methane/hydrogen/air laminar premixed flames at atmospheric pressure: Effect of hydrogen addition to fuel on soot gaseous precursors, Int. J. Hydrogen Energy 41 (2016) 6929-6942.
[30] C. Betrancourt, F. Liu, P. Desgroux, X. Mercier, A. Faccinetto, M. Salamanca, L. Ruwe, K. Kohse-Höinghaus, D. Emmrich, A. Beyer, A. Gölzhäuser, T. Tritscher, Investigation of the size of the incandescent incipient soot particles in premixed sooting and nucleation flames of n-butane using LII, HIM, and 1 nm-SMPS, Aerosol Science and Technology 51 (2017) 916-935.
[31] C. Irimiea, A. Faccinetto, X. Mercier, I.-K. Ortega, N. Nuns, E. Therssen, P. Desgroux, C. Focsa, Unveiling trends in soot nucleation and growth: When secondary ion mass spectrometry meets statistical analysis, Carbon 144 (2019) 815-830.
[32] K. Gleason, F. Carbone, A.J. Sumner, B.D. Drollette, D.L. Plata, A. Gomez, Small aromatic hydrocarbons control the onset of soot nucleation, Combust. Flame 223 (2021) 398-406.
[33] K. Gleason, F. Carbone, A. Gomez, PAHs controlling soot nucleation in 0.101—0.811MPa ethylene counterflow diffusion flames, Combust. Flame 227 (2021) 384-395.
[34] The International Sooting Flame (ISF) Workshop, (2021).
[35] H. Mätzing, H.G. Wagner, Measurements about the influence of pressure on carbon formation in premixed laminar C2H4-air flames, Symposium (International) on Combustion 21 (1988) 1047-1055.
[36] B. Bohm, J. Brubach, C. Ertem, A. Dreizler, Experiments for combustion-LES validation, Flow Turbul. Combust. 80 (2008) 507-529.
[37] M.M. Maricq, Size and charge of soot particles in rich premixed ethylene flames, Combust. Flame 137 (2004) 340-350.
[38] L.A. Sgro, A. De Filippo, G. Lanzuolo, A. D'Alessio, Characterization of nanoparticles of organic carbon (NOC) produced in rich premixed flames by differential mobility analysis, Proc. Combust. Inst. 31 (2007) 631-638.
[39] F. Goebel, C. Mundt, Implementation of the P1 Radiation Model in the CFD solver NSMB and Investigation of Radiative Heat Transfer in the SSME Main Combustion Chamber, 17th AIAA International Space Planes and Hypersonic Systems and Technologies Conference.
[40] S.J. Brookes, J.B. Moss, Predictions of soot and thermal radiation properties in confined turbulent jet diffusion flames, Combust. Flame 116 (1999) 486-503.
[41] J. Appel, H. Bockhorn, M. Frenklach, Kinetic modeling of soot formation with detailed chemistry and physics: laminar premixed flames of C2 hydrocarbons, Combust. Flame 121 (2000) 122-136.
[42] D.M.G. Gregory P. Smith, Michael Frenklach, Nigel W. Moriarty, Boris Eiteneer, Mikhail Goldenberg, C. Thomas Bowman, Ronald K. Hanson, Soonho Song, William C. Gardiner, Jr., Vitali V. Lissianski, and Zhiwei Qin, GRI-MECH 3.0.
[43] M. Frenklach, Method of moments with interpolative closure, Chemical Engineering Science 57 (2002) 2229-2239.
[44] H. Guo, K.A. Thomson, G.J. Smallwood, On the effect of carbon monoxide addition on soot formation in a laminar ethylene/air coflow diffusion flame, Combust. Flame 156 (2009) 1135-1142.

[45] S. De Iuliis, S. Maffi, F. Migliorini, F. Cignoli, G. Zizak, Effect of hydrogen addition on soot formation in an ethylene/air premixed flame, Appl. Phys. B 106 (2012) 707-715.
[46] F. Liu, Y. Ai, W. Kong, Effect of hydrogen and helium addition to fuel on soot formation in an axisymmetric coflow laminar methane/air diffusion flame, Int. J. Hydrogen Energy 39 (2014) 3936-3946.
[47] Z. Wang, J. Yang, Z. Li, Y. Xiang, Syngas composition study, Frontiers of Energy and Power Engineering in China 3 (2009) 369-372.
[48] C. Renard, P.J. Van Tiggelen, J. Vandooren, Effect of dimethoxymethane addition on the experimental structure of a rich ethylene/oxygen/argon flame, Proc. Combust. Inst. 29 (2002) 1277-1284.
[49] H. Guo, F. Liu, G.J. Smallwood, Ö.L. Gülder, The flame preheating effect on numerical modelling of soot formation in a two-dimensional laminar ethylene–air diffusion flame, Combustion Theory and Modelling 6 (2002) 173-187.
[50] T.S. Wang, R.A. Matula, R.C. Farmer, Combustion kinetics of soot formation from toluene, Symposium (International) on Combustion 18 (1981) 1149-1158.

SUPPLEMENTAL MATERIAL

Author version accompanying the accepted manuscript

Influence of lateral species diffusion and heat transfer on the evaluation of near-threshold sooting flames: Supplemental material

Ahmad Saylam, Torsten Endres, Christof Schulz

EMP, Institute for Energy and Materials Processes – Reactive Fluids, and CENIDE, Center for Nanointegration Duisburg-Essen, University of Duisburg-Essen, Duisburg, Germany

A: Experiment description

The measurement of soot volume fraction f_V in the slightly sooting premixed ethylene/air flame $\phi = 2.1$ was described in a previous work of our lab by Mi el al. [1] using three-pass extinction (3PE). The burner was enclosed in a vessel for studying high-pressure flames. The burner matrix for the target flame has a diameter of 20 mm, which is surrounded by a ring-shaped matrix with an outer diameter of 56 mm to operate a non-sooting premixed methane/air flame $\phi = 1.2$. The latter is surrounded by another ring-shaped matrix with an outer diameter of 86 mm to deliver an air co-flow (cf., Fig. S1) to stabilize the flames against buoyancy effects, shield the hot gases from burner walls and windows and cool the exhaust gases. This burner is also used to conduct measurements of f_V by cavity ring-down extinction (CRDE) in the absence of the pressure vessel and windows and installing a stagnation plate of 40 mm diameter at HAB = 35 mm. The CRDE measurements were performed with an optical setup almost identical to the one described in Betrancourt et al. [2].

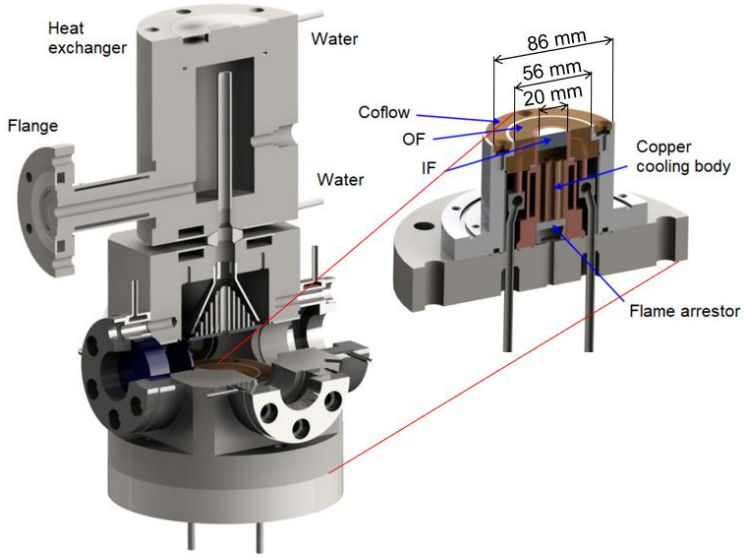

Figure S1. Drawing of the burner used to conduct the f_V measurements in ethylene/air flames: For three-pass extinction the burner as shown on the left was used; for the CRDE-measurements the burner shown as an inset on the right was removed from the pressure vessel and operated without windows.

B: Simulation capability for near-threshold sooting flames

B.1 Ethylene/air flame

The achievement of significant modeling results and trusted perspective passes indeed by a validation process of the applied simulation approach results against experimental data. Therefore, the step I in the investigation strategy of this work, presented in paper introduction, is the proving of enough good prediction level of the employed combustion mechanisms of ethylene/air mixture of Appel et al. [3], as well as the performance of the executed 2D simulations using Fluent under Ansys to predict the experimental data of Carbone et al. [4]. Figure S2 shows a comparison between the measured axial temperature profile using a silica-coated R-type thermocouple in a burner diameter of 48 mm [4] and the 2D simulated ones of the nearby burner configurations N40 and N60, cf. Table 2. Both predicted temperature profiles of N40 and N60 are in good agreement with the experimental data; the divergence between the simulated and experimental data is in the range of measurement error, up to 94 K [4].

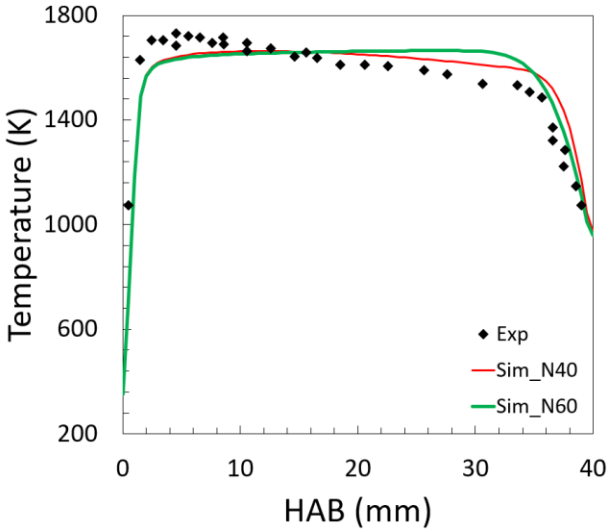

Figure S2. Comparison between the measured axial temperature profile [4] (symbols) and the 2D simulated ones (lines) of the atmospheric ethylene/air flame of ϕ = 2.1.

The simulations of the two burner configurations N40 and N60 to predict the experimental axial profiles of CO, H_2, CH_4, C_4H_4, C_2H_2, C_6H_6, naphthalene, and f_V of Carbone et al. [4] are presented in figure S3. The f_V were measured using a light extinction (LE) and pyrometry (Py) techniques. The measured f_V by three-pass extinction approach (3PE) of Mi el al. [1] and those done in this work by CRDE diagnostic are also added into figure S3h for comparison. The selection of CO and H_2 species is due to their effect on soot formation process [5-8] and those of C_4H_4, C_2H_2, C_6H_6, and naphthalene to their role as soot precursors.

The simulation predicts relatively well the axial profiles of CO, H_2, C_2H_2, and C_4H_4. The trend of the simulated axial profiles of methane, naphthalene and f_V is in good agreement with the experimental data. The prediction of benzene is relatively poor. The divergence in species and soot production between experience and prediction using the both burner diameters of 40 and 60 mm (Sim_N40 and Sim_N60) is very narrow for the most of species with an exception of hydrogen as a high reactivity and diffusivity specie, and thus it shows higher sensitivity to the lateral influence regarding the other species. The Moss-Brookes model of soot formation implemented in 2D simulation [9] overestimates highly the experimental f_V data. Nevertheless, the tendency of the axial profile of all the experimental f_V data is well reproduced by the simulation.

B.2 Methane/O_2/N_2 flame

The ϕ = 1.82 $CH_4/O_2/N_2$ atmospheric premixed flame of Do et al. [10] is simulated realizing 2D simulation of an axisymmetric flame of Fluent under Ansys employing the mechanisms of GRI-3.0 [11, 12]. A correction to the measured axial profile of temperature by Do et al. [10] is done using the approach of Hindasageri et al. [13]. Figure S4 shows a comparison between the experimental temperature profile of a thermocouple measurement with and without correction (Exp_WK and Exp_NK), and the temperatures resulting from the 2D simulations. The simulation predicts modestly the height of the flame preheating zone but with higher temperatures of burned gases, which are closer to those of adiabatic flame. Depending on HAB, the experimental temperatures increase by 0.5 and 44 K after radiation correction. 2D simulations of burner configuration N60 were conducted to predict the experimental axial profiles of CH_4, C_2H_2, O_2, H_2, CO, CO_2, H_2O, and f_V presented in Figure S5.

The experimental consumption rates (i.e., the slopes of the respective concentration profiles) of methane and oxygen, shown in figure S5a–b, are much lower than those predicted by the simulations. The experimental full consumption of fuel and oxygen is attained at HAB = 12 mm, which is shifted by about 4–6 mm downstream with respect to predictions from the simulation. This important difference in consumption rate between experiment and simulation of fuel and O_2 will affect indeed the spatial formation of all the studied species presented in Figures S5c–g. The simulation predicts relatively well the production rate of syngas (CO and H_2), H_2O and C_2H_2, only at the exist of the burner (high HABs). However, the simulation shows the same trends as the experiment in function of HAB. The 2D simulation using the Moss-Brookes model overestimates highly the experimental f_V.

Since the chemistry could not predict the experimental temperature and species profiles well enough, but could predict experimental trends of f_V versus HABs for this nucleation flame, the simulation outcome of this work can therefore only be considered as a compass indicator for perspective investigations.

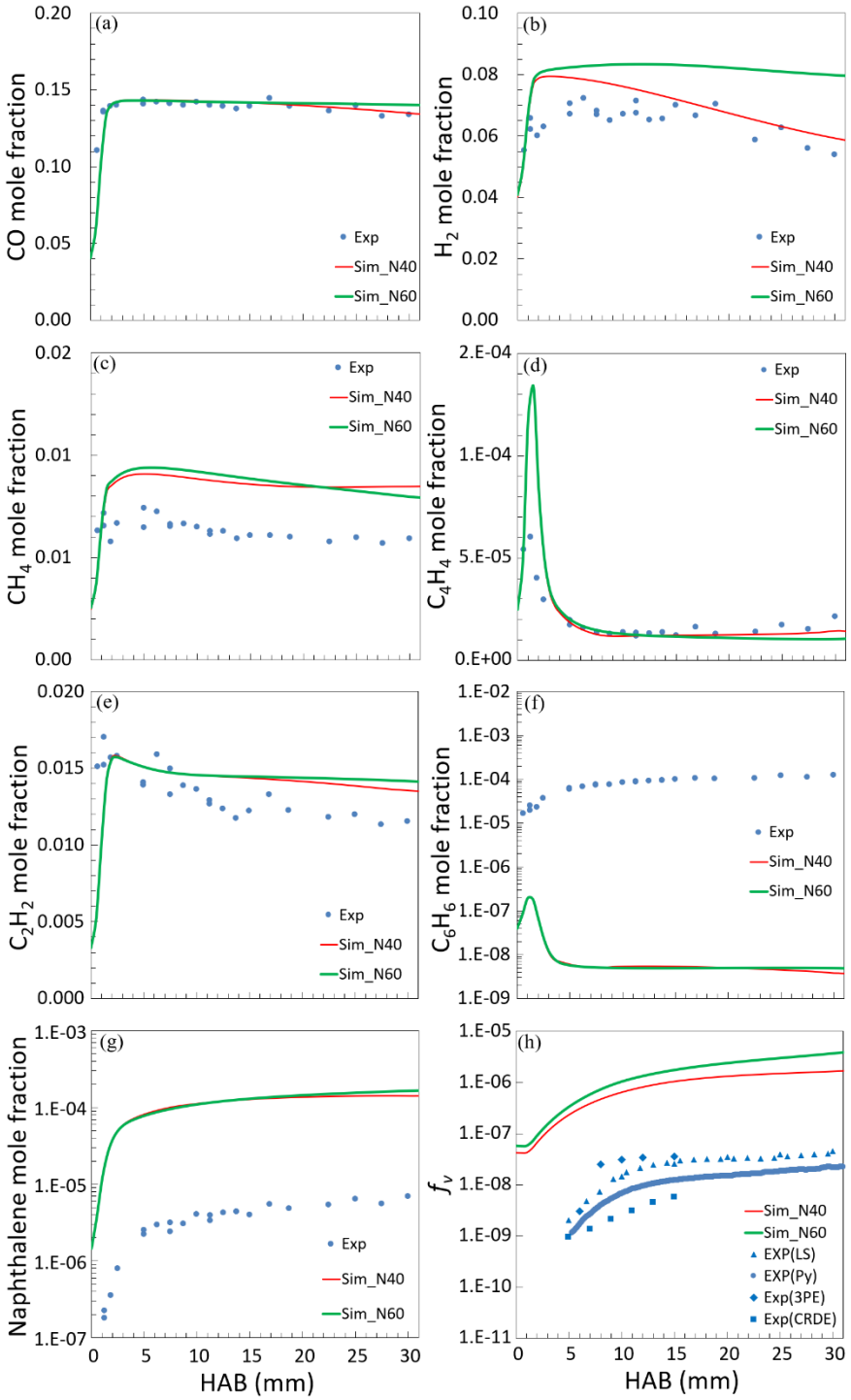

Figure S3. Experimental Exp(Py&LS) [4, 14], Exp(3PE) [1] and this work Exp(CRDE), and simulated axial profiles of species mole fraction (a: CO, b: H_2, c: CH_4, d: C_4H_4, e: C_2H_2, f: C_6H_6, g: naphthalene) and h: f_V vs. HAB of ϕ = 2.1 C_2H_4/air atmospheric pressure premixed flame.

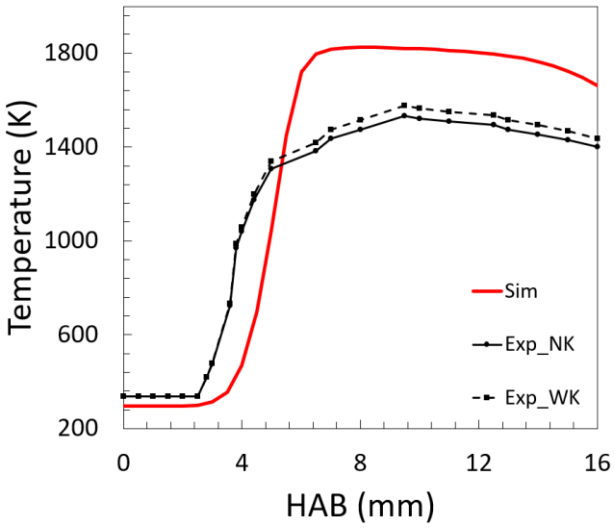

Figure S4. Comparison between the experimental axial temperature profiles from Do et al. [10] without (black solid line with symbols) and with (black dashed line with symbols) heat transfer correction, and results from 2D simulations.

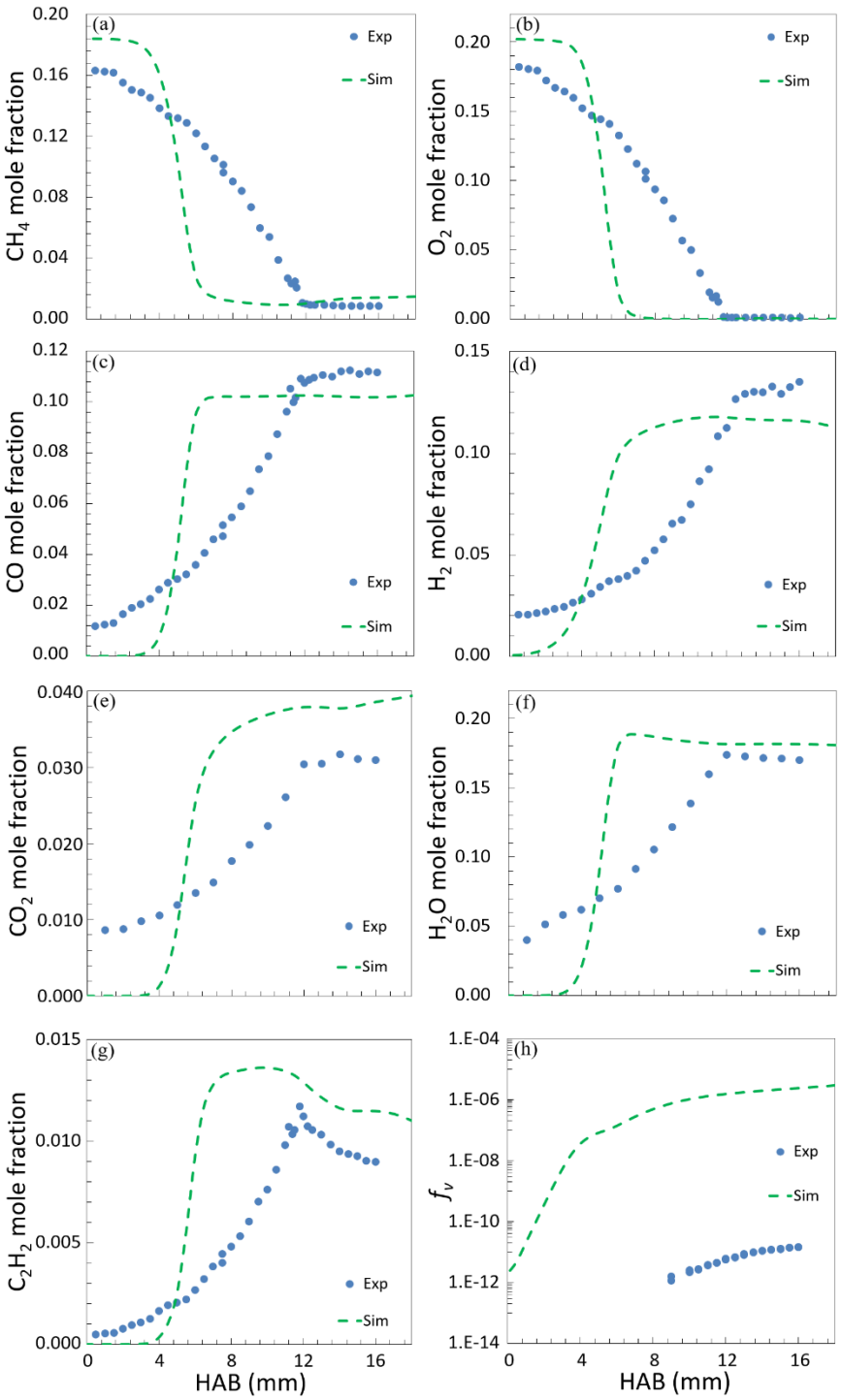

Figure S5. Experimental (Exp) of Do et al. [10] and predicted (Sim) species mole fraction (a: CH_4, b: O_2, c: CO, d: H_2, e: CO_2, f: H_2O and g: C_2H_2) and h: f_V profiles vs HAB of ϕ = 1.82 $CH_4/N_2/O_2$ atmospheric premixed flame.

References

[1] X. Mi, A. Saylam, T. Endres, C. Schulz, T. Dreier, Near-threshold soot formation in premixed flames at elevated pressure, Carbon 181 (2021) 143-154.

[2] C. Betrancourt, X. Mercier, F. Liu, P. Desgroux, Quantitative measurement of volume fraction profiles of soot of different maturities in premixed flames by extinction-calibrated laser-induced incandescence, Appl. Phys. B 125 (2019) 16.

[3] J. Appel, H. Bockhorn, M. Frenklach, Kinetic modeling of soot formation with detailed chemistry and physics: laminar premixed flames of C2 hydrocarbons, Combust. Flame 121 (2000) 122-136.

[4] F. Carbone, K. Gleason, A. Gomez, Probing gas-to-particle transition in a moderately sooting atmospheric pressure ethylene/air laminar premixed flame. Part I: gas phase and soot ensemble characterization, Combust. Flame 181 (2017) 315-328.

[5] H. Guo, K.A. Thomson, G.J. Smallwood, On the effect of carbon monoxide addition on soot formation in a laminar ethylene/air coflow diffusion flame, Combust. Flame 156 (2009) 1135-1142.

[6] S. De Iuliis, S. Maffi, F. Migliorini, F. Cignoli, G. Zizak, Effect of hydrogen addition on soot formation in an ethylene/air premixed flame, Appl. Phys. B 106 (2012) 707-715.

[7] F. Liu, Y. Ai, W. Kong, Effect of hydrogen and helium addition to fuel on soot formation in an axisymmetric coflow laminar methane/air diffusion flame, Int. J. Hydrogen Energy 39 (2014) 3936-3946.

[8] Z. Wang, J. Yang, Z. Li, Y. Xiang, Syngas composition study, Frontiers of Energy and Power Engineering in China 3 (2009) 369-372.

[9] S.J. Brookes, J.B. Moss, Predictions of soot and thermal radiation properties in confined turbulent jet diffusion flames, Combust. Flame 116 (1999) 486-503.

[10] H.-Q. Do, L.-S. Tran, L. Gasnot, X. Mercier, A. El Bakali, Experimental study of the influence of hydrogen as a fuel additive on the formation of soot precursors and particles in atmospheric laminar premixed flames of methane, Fuel 287 (2021) 119517.

[11] D.M.G. Gregory P. Smith, Michael Frenklach, Nigel W. Moriarty, Boris Eiteneer, Mikhail Goldenberg, C. Thomas Bowman, Ronald K. Hanson, Soonho Song, William C. Gardiner, Jr., Vitali V. Lissianski, and Zhiwei Qin, GRI-MECH 3.0.

[12] C. Saggese, S. Ferrario, J. Camacho, A. Cuoci, A. Frassoldati, E. Ranzi, H. Wang, T. Faravelli, Kinetic modeling of particle size distribution of soot in a premixed burner-stabilized stagnation ethylene flame, Combust. Flame 162 (2015) 3356-3369.

[13] V. Hindasageri, R.P. Vedula, S.V. Prabhu, Thermocouple error correction for measuring the flame temperature with determination of emissivity and heat transfer coefficient, Rev. Sci. Instrum. 84 (2013) 024902.

[14] W. Pejpichestakul, A. Cuoci, A. Frassoldati, M. Pelucchi, A. Parente, T. Faravelli, Buoyancy effect in sooting laminar premixed ethylene flame, Combust. Flame 205 (2019) 135-146.